

Strange Metal Analog in a Fermi Lattice Gas

W. Xu, W. McGehee,* W. Morong, and B. DeMarco[†]

Department of Physics, University of Illinois at

Urbana-Champaign, Urbana, Illinois 61801, USA

(Dated: July 28, 2022)

Abstract

Strange metals have defied explanation since they were discovered nearly 30 years ago as the normal state of strongly correlated high-temperature superconductors. In these materials, which cannot be described using Fermi liquid theory, the resistance scales anomalously with temperature, and the lifetime of single-particle momentum states is sufficiently short for the particles to lose their individual character. A microscopic theory and the necessary ingredients for these behaviors are unknown. Here, we report a new method that uses stimulated Raman transitions to create momentum excitations and measure their lifetime in the metallic regime of an optical lattice Hubbard model, which is a minimal paradigm for strongly correlated electronic solids. We discover two signatures of strange metals by measuring the momentum relaxation time at varied interaction strengths and temperatures. First, the lifetime at low temperature and the highest interaction strength is comparable to the tunneling time, making the excitation strongly incoherent. Second, the lifetime decreases with temperature, in complete opposition to a kinetic theory prediction and the generic behavior of trapped atomic gases. We show that this behavior can be interpreted as a temperature-dependent collision cross section that nearly achieves the hard-sphere limit associated with the lattice.

*now at: Center for Nanoscale Science and Technology, National Institute of Standards and Technology, Gaithersburg, Maryland 20899, USA

[†]Electronic address: bdemarco@illinois.edu

Landau’s Fermi liquid theory successfully describes the behavior of interacting fermionic particles for a wide range of materials, such as electrons in simple metals and liquid helium-3 [1]. In this scenario, quasiparticles with renormalized dispersion incorporate the influence of interactions and determine properties such as resistance. Fermi liquid theory fails when strong correlations or fluctuations are present [2], such as in the metallic state in high-temperature cuprate superconductors. Also known as strange metals, these states present anomalous properties such as resistance that depends linearly on temperature T , contrary to the T^2 prediction of Fermi liquid theory [2, 3]. There is strong evidence that strange metals cannot be described using quasiparticles [4]—the resistivity does not saturate as temperature is increased [5] and particle-like excitations are absent in photoemission spectroscopy [6].

Theories and phenomenological descriptions for understanding strange metals remain controversial [7–9]. A central challenge is understanding the parameters that control and determine the relaxation time for momentum-carrying excitations, which is connected to the imaginary part of the self energy and is the fundamental quantity that determines resistivity [1]. In material systems, the lifetime of excitations is determined by scattering from sources such as disorder, phonons, and between quasiparticles. If the relaxation time becomes comparable to dynamic timescales in the system, such as the tunneling time, then the assumption in Fermi liquid theory that the interactions can be turned on adiabatically is violated. In this “incoherent” regime, momentum-carrying excitations lose their individual identity because they dissipate so rapidly such that the fundamental assumptions underlying the quasiparticle picture break down [1, 10, 11].

Ultracold fermionic atoms trapped in optical lattices, which realize the Fermi-Hubbard model [12–14], provide a well-controlled platform free of phonons and impurities to study strange metal phenomenology and to identify the minimal ingredients required to generate these behaviors. In ultracold gas experiments with fermionic atoms, photoemission spectroscopy has been used to indirectly probe the momentum relaxation time in the BEC–BCS crossover for a trapped gas, and a failure of Fermi liquid theory was discovered [15]. Transport measurements such as diffusion in a 2D lattice gas [16], shear viscosity in a unitary Fermi gas [17], and spin diffusion [18] have also probed the effect of strong interactions on various relaxation processes. In this paper, we describe a method for directly measuring the lifetime for momentum excitations in a two-component fermionic gas composed of ^{40}K atoms trapped in a cubic optical lattice. Quasimomentum excitations are created using stimulated

Raman transitions (Fig. 1), and the relaxation time is determined by fully resolving the decay of the excitations. Our measurements suggest that solely on-site inter-particle interactions are sufficient to produce behavior analogous to that of a strange metal in a strongly correlated lattice model.

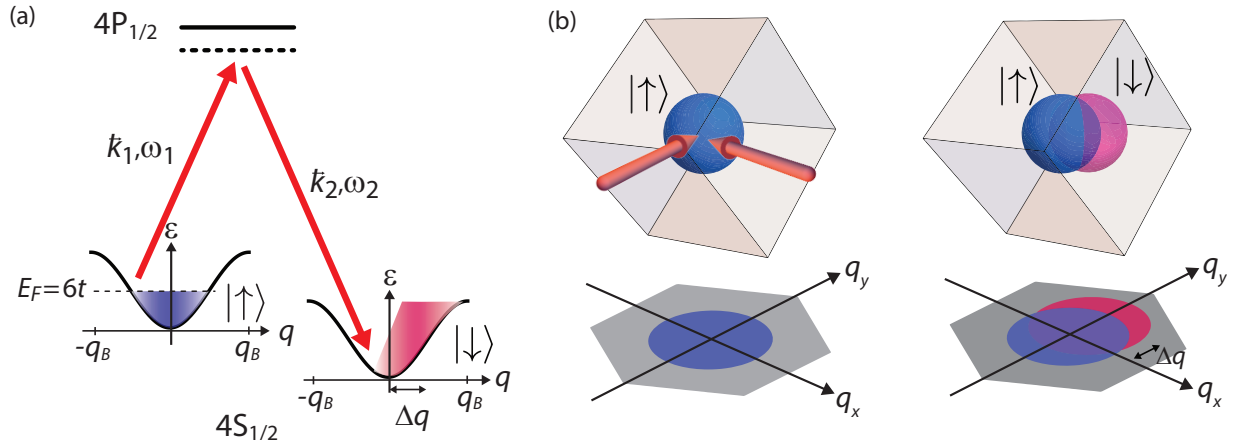


FIG. 1: Schematic diagram of momentum excitation created via Raman transition. (a) A spin-polarized $|\uparrow\rangle$ (blue) gas is prepared in a metallic state in the ground band (with dispersion ϵ) of the lattice. A pair of Raman beams (red arrows) with frequencies ω_1, ω_2 and wavevectors \vec{k}_1, \vec{k}_2 are used to quickly transfer atoms from the $|\uparrow\rangle$ to the $|\downarrow\rangle$ (red) state via the $4S_{1/2} \rightarrow 4P_{1/2}$ electronic transition. The frequency difference $\delta\omega = \omega_1 - \omega_2$ is tuned to be resonant, and the Raman pulse almost equally samples all quasimomenta q in the Brillouin zone, which ranges along one direction from $-q_B$ to $q_B = \hbar\pi/d$, where $d \approx 390$ nm is the lattice spacing. The Raman transition introduces a momentum shift Δq for the atoms in the $|\downarrow\rangle$ state. (b) The quasimomentum distribution in 3D Brillouin zone is shown before (left) and after (right) the Raman pulse. The initial quasimomentum shift has approximate magnitude $0.5 q_B$ and is aligned with the direction of q_y and $\vec{\delta k}$, which is along the $[-1, -1, 1]$ direction. The imaging procedure projects the quasimomentum distributions along the $[1, 1, 1]$ direction, so that the Brillouin zone has a hexagonal shape in the imaging plane, which has axes q_x and q_y .

We prepare the gas in a metallic state by slowly superimposing the optical lattice after cooling in an optical dipole trap to temperatures $T \approx 0.2\text{--}1.2 T_F$, where $E_F = k_B T_F$ is the Fermi energy. The temperature of the gas is sufficiently low for the atoms to realize a single-band Hubbard model described by the Hamiltonian $H = -t \sum_{\langle i,j \rangle, \sigma} (\hat{c}_{j\sigma}^\dagger \hat{c}_{i\sigma} + h.c.) +$

$U \sum_i n_{i,\downarrow} n_{i,\uparrow} + \sum_{i,\sigma} m\omega^2 r_i^2 n_{i,\sigma} / 2$, where i indexes the lattice sites, $\langle \rangle$ indicates a sum over neighboring sites, $\sigma = \uparrow, \downarrow$ indexes spin, ω is the geometric mean of the dipole trap frequencies, r_i is the distance from site i to the trap center, c_i^\dagger (c_i) creates (annihilates) an atom from site i , $n_{i,\sigma} = c_i^\dagger c_i$ is the number operator, t is the Hubbard tunneling energy, and U is the on-site Hubbard interaction energy [12]. Two hyperfine states $|F = 9/2, m_F = 9/2\rangle$ ($|\uparrow\rangle$) and $|F = 9/2, m_F = 7/2\rangle$ ($|\downarrow\rangle$) play the role of the electron spin. The metallic regime is achieved by tuning the number of atoms N so that $E_F \approx 6t$ (i.e., 0.5 particles of each spin per site in the center of the lattice at $T = 0$) and the lattice potential depth s to sample $U/t \approx 2.3$ –9.0. The interactions between particles cannot be accommodated in theory perturbatively for this range of interaction strengths. Therefore, to create a well characterized initial state, the gas is spin polarized by removing the $|\downarrow\rangle$ atoms before turning on the lattice. Using a spin-polarized, non-interacting gas enables accurate knowledge of the quasimomentum and density distributions before an excitation is generated, because this model has an exact solution when interactions are absent [19, 20]. We use this solution, measurements of N and T , and a straightforward application of the adiabatic theorem of quantum mechanics to estimate an effective chemical potential $\tilde{\mu}$ and temperature \tilde{T} of the initial metallic lattice gas [21]. These parameters are used in a weak-scattering kinetic calculation of the relaxation rate [21].

Momentum excitations consisting of approximately 30% of the atoms transferred to the $|\downarrow\rangle$ state are created using a pulse of two laser beams focused onto the gas (Fig. 1). The quasimomentum profiles of the atoms in the $|\uparrow\rangle$ and $|\downarrow\rangle$ states are separately imaged after evolution time t_{hold} in the lattice using bandmapping [20] and spin-resolved time-of-flight imaging [21]. Sample images for $s = 4E_R$, corresponding to $U/t = 2.3$, and $T/T_F = 0.23$ before turning on the lattice ($k_B \tilde{T} = 1.3t$) are shown in Fig. 2a. The quasimomentum distribution of the $|\uparrow\rangle$ gas is unaffected by the Raman pulse, while the $|\downarrow\rangle$ gas is displaced along the wavevector difference $\delta\vec{k} = \vec{k}_1 - \vec{k}_2$ between the Raman beams.

The decay of the excitation caused by momentum-changing collisions between atoms in $|\downarrow\rangle$ and $|\uparrow\rangle$ states is apparent in images taken for different evolution times in the lattice following the Raman pulse. The excitation, visible in images formed by subtracting the equilibrium $|\downarrow\rangle$ quasimomentum distribution (Fig 2b), dissipates within a few milliseconds as the $|\downarrow\rangle$ component motion relaxes. Effects besides interactions play a minor role in the excitation dynamics. The relaxation is too fast for the trap forces to play a significant part in

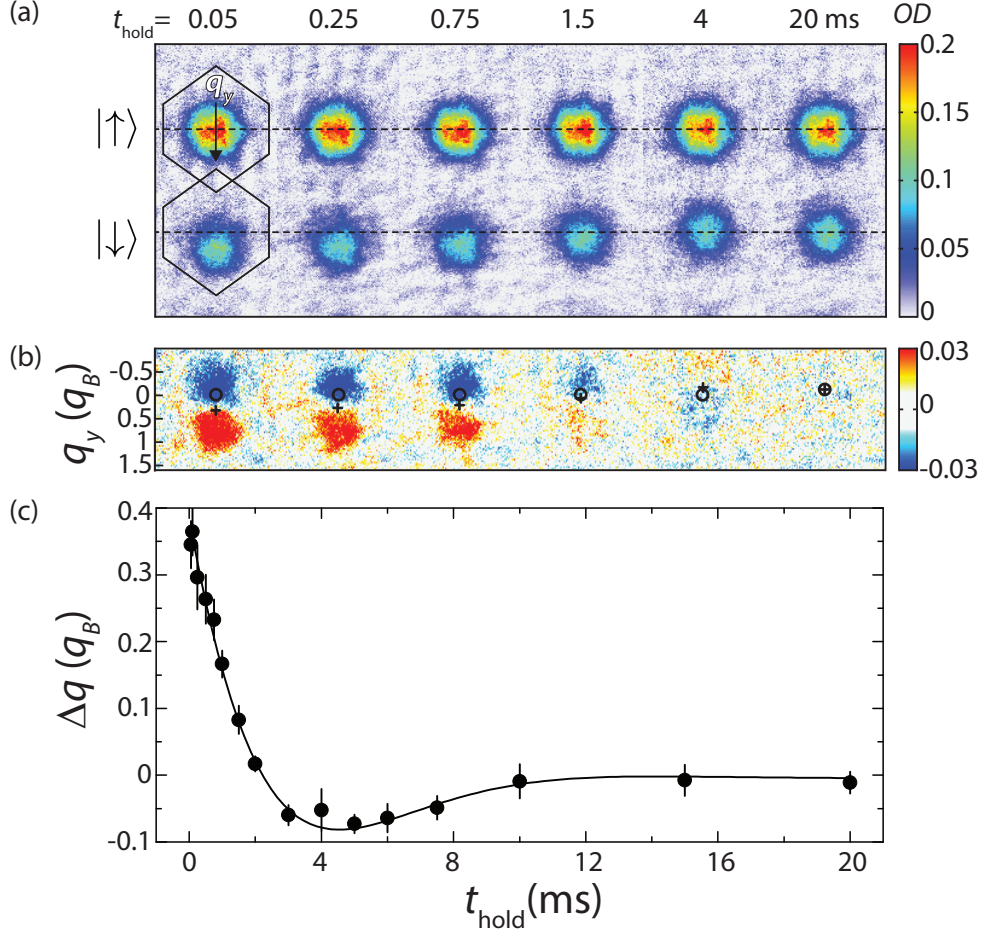


FIG. 2: (a) Quasimomentum distribution for the $|\uparrow\rangle$ and $|\downarrow\rangle$ components for different evolution times after the Raman pulse for $T/T_F = 0.23$ and $U/t = 2.3$ ($s = 4E_R$). The dashed lines mark $q = 0$, and the hexagons are the first Brillouin zone (BZ) projected onto the imaging plane. The color bar shows the measured optical depth (OD). Fits to these quasimomentum profiles are used to determine the momentum of the excitation Δq [21]. (b) Images of the excitation produced by subtracting the quasimomentum profile of the $|\downarrow\rangle$ component from the equilibrium profile measured at $t_{\text{hold}} = 20$ ms with a spin-mixed gas subjected to a Raman pulse far from resonance. For these images, only the BZ for the $|\downarrow\rangle$ component is shown. The cross indicates the center of the $|\downarrow\rangle$ component for each t_{hold} , and the circle marks the center of the equilibrium distribution. (c) The momentum of the excitation for different evolution times is fit (solid line) to a model of linear dissipation to determine the relaxation time constant. Each point is the average of 5–10 measurements, and the error bars show the standard error of the mean.

the dynamics or for the motion of the $|\uparrow\rangle$ atoms to be affected for most of the temperatures and interaction strengths we sample. We have also checked that dephasing of atomic trajectories with different initial quasimomenta does not significantly contribute to the relaxation via classical dynamics simulations and measurements employing spin-polarized gases [21]. Furthermore, using semi-classical, non-interacting thermodynamics, we estimate that the kinetic energy of the excitation increases the temperature of the gas by less than 5%.

We measure the characteristic relaxation time by fitting the excitation dynamics to a model of linear dissipation. The quasimomentum of the excitation Δq for each evolution time is determined by fitting the image of each spin component to a Gaussian function [21]. Sample data corresponding to the images in Fig. 2a are shown in Fig. 2c. To determine the relaxation time τ , the data are fit to a model that describe the motion of the atoms in response to the trap and a frictional force that relaxes the relative momentum between spin components [21–23]. For a weakly interacting, harmonically trapped gas, the frictional force is proportional to the collision rate per atom. The τ determined by this method is the analog of the relaxation time in the Drude model for resistivity and the inverse linewidth of the spectral function. Measurements of τ for different interaction strengths and temperatures are shown in Fig. 3.

As a baseline for understanding, we compare measurements of τ with a kinetics calculation that accounts for atoms scattering between quasimomentum states. This technique has been used to accurately calculate relaxation times for trapped gases in the weakly interacting regime [22]. Based on general principles, this approach predicts that τ decreases for stronger interactions, since the rate of scattering events increases, and that τ increases at higher temperatures, because the density is reduced. Furthermore, while Pauli blocking limits the phase space for scattering and causes the equilibrium collision rate to vanish at zero temperature [22], τ for our measurement remains finite at $T = 0$ because the excitation creates unfilled quantum states. The band structure introduced by the lattice changes this picture only quantitatively by modifying the dispersion, which changes the constraints on energy and momentum conservation and limits the range of available kinetic energy. The impact of the strong Hubbard interactions between atoms induced by the lattice is, however, not understood, and calculating relaxation rates, conductivity, and diffusion constants is an outstanding challenge.

The results of a weak-scattering kinetic theory calculation, obtained via Enskog’s equa-

tion of change [24] and by treating the Hubbard interaction as a perturbation to the band structure using Fermi's Golden Rule, are shown with the data in Fig. 3. The calculation has no free parameters, fully accounts for the trap and quantum statistics, and averages over a thermodynamic distribution of quasimomenta based on the inferred \tilde{T} and $\tilde{\mu}$. For the interaction strength dependence measurements shown in Fig. 3a, $U/t = 2.3\text{--}9$ is tuned at fixed $T/T_F \approx 0.25$ by changing the lattice potential depth from $s = 4\text{--}7 E_R$. With E_F fixed to approximately $6t$, the kinetic calculation predicts $\tau \propto t/U^2$ [21]. Behavior close to this scaling is evident in Fig. 3a, which shows the measured τ scaled by the tunneling time \hbar/t for different s . The normalized relaxation rate speeds up with increasing interaction strength, decreasing by approximately a factor of six. The quantitative agreement at low s is surprising given that $U > t$, and therefore the weak-scattering approximation may be invalidated.

In contrast to the qualitative agreement apparent in Fig. 3a, the temperature dependence of τ shown in Fig. 3b shows a trend opposite to that predicted by kinetic theory. For these data, we fix the interaction strength to $U/t = 2.3$ (corresponding to $s = 4 E_R$) and vary the temperature of the gas before turning on the lattice from $T/T_F \approx 0.2\text{--}1.2$, which leads to $k_B\tilde{T}/t \approx 1\text{--}8$. The measured time constant agrees with kinetic theory at the lowest temperatures. As the temperature is increased, τ decreases by approximately a factor of two, while the kinetic calculation predicts that τ increases by a factor of 2.5, leading to a disagreement of over 20 standard errors at the highest temperature. This discrepancy cannot be explained by an error in density—we have verified that the density of the gas decreases across this range and is consistent with thermodynamic calculations via in-situ imaging [21]. Furthermore, the kinetic theory prediction is insensitive to errors in \tilde{T} and $\tilde{\mu}$.

Two prominent features of the data shown in Fig.3 are reminiscent of strange metal phenomena: incoherent behavior and faster relaxation at higher temperatures. Transport in a metal becomes incoherent when states with definite momentum are short lived compared with single-particle and excitation timescales [25], an effect that we observe for the low T/T_F data shown in Fig. 3a. The shortest excitation lifetimes we measure occur at the largest U/t , where τ is approximately equal to the tunneling time \hbar/t , which is the characteristic single-particle timescale. This commensurability of timescales signals incoherent behavior and a breakdown of the central assumption underlying Fermi liquid theory.

Relaxation times naturally decrease and resistivity increases in metals at higher tempera-

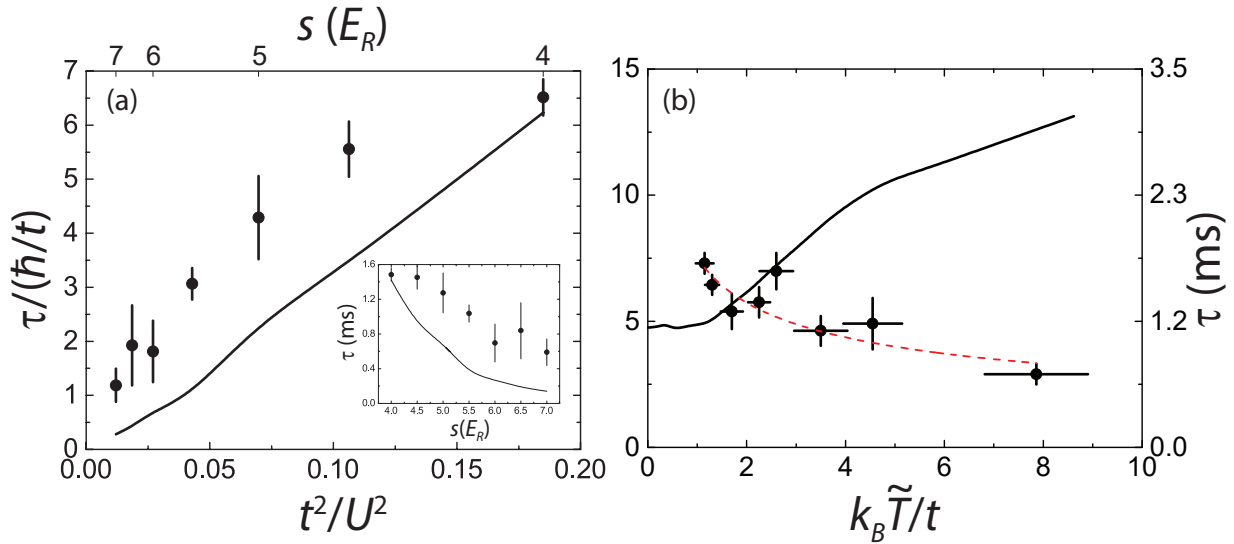


FIG. 3: (a) Interaction strength dependence of the relaxation time. The inset shows the measured τ determined from fits to data such as those shown in Fig. 2c. Relaxation accelerates as the interaction strength increases, with τ reaching the tunneling time \hbar/t at $t/U \approx 0.11$. (b) Temperature dependence of the relaxation time. The red-dashed line shows a power-law fit. In both plots, the measurements are compared with a weak-scattering kinetics calculation (solid line). For (a), the average value of \tilde{T} and $\tilde{\mu}$ are used in the calculation, while in (b), we take the average value of N . The vertical error bars show the uncertainty in the fit used to determine τ , and the horizontal error bars in (b) show the uncertainty in T from TOF thermometry.

tures. In strange metals, the resistivity is large and increases more rapidly with temperature than predicted by Fermi liquid and kinetic theory. The decrease in τ evident in Fig. 3b is a similar but even more striking phenomenon, since τ is predicted to increase at higher temperatures for any trapped gas. A microscopic theory that successfully describes these kind of phenomena has not been developed. Several approaches, including marginal Fermi liquid phenomenology [26] and effective theories such as AdS/CFT duality [27, 28], have provided different predictions for how τ scales with T in strange metals. The power-law fit shown in Fig. 3b with $\tau \propto \tilde{T}^{(-0.39 \pm 0.08)}$ cannot be compared directly with these predictions for solids, however, since the density is inhomogeneous and varies with temperature.

While a theory for the behavior in Fig. 3b is unavailable, it is natural to interpret the relaxation time for trapped atomic gases in terms of a collision cross section σ . In the semi-classical limit, $\tau = n_{dwd} \sigma v_{rel} / N_{\downarrow}$, where n_{dwd} is the density-weighted density, and

v_{rel} is the mean relative speed between colliding partners [21, 29]. We show σ in Fig. 4 determined using the measured τ from Fig. 3b and inferring n_{dwd} and v_{rel} from semi-classical thermodynamics.

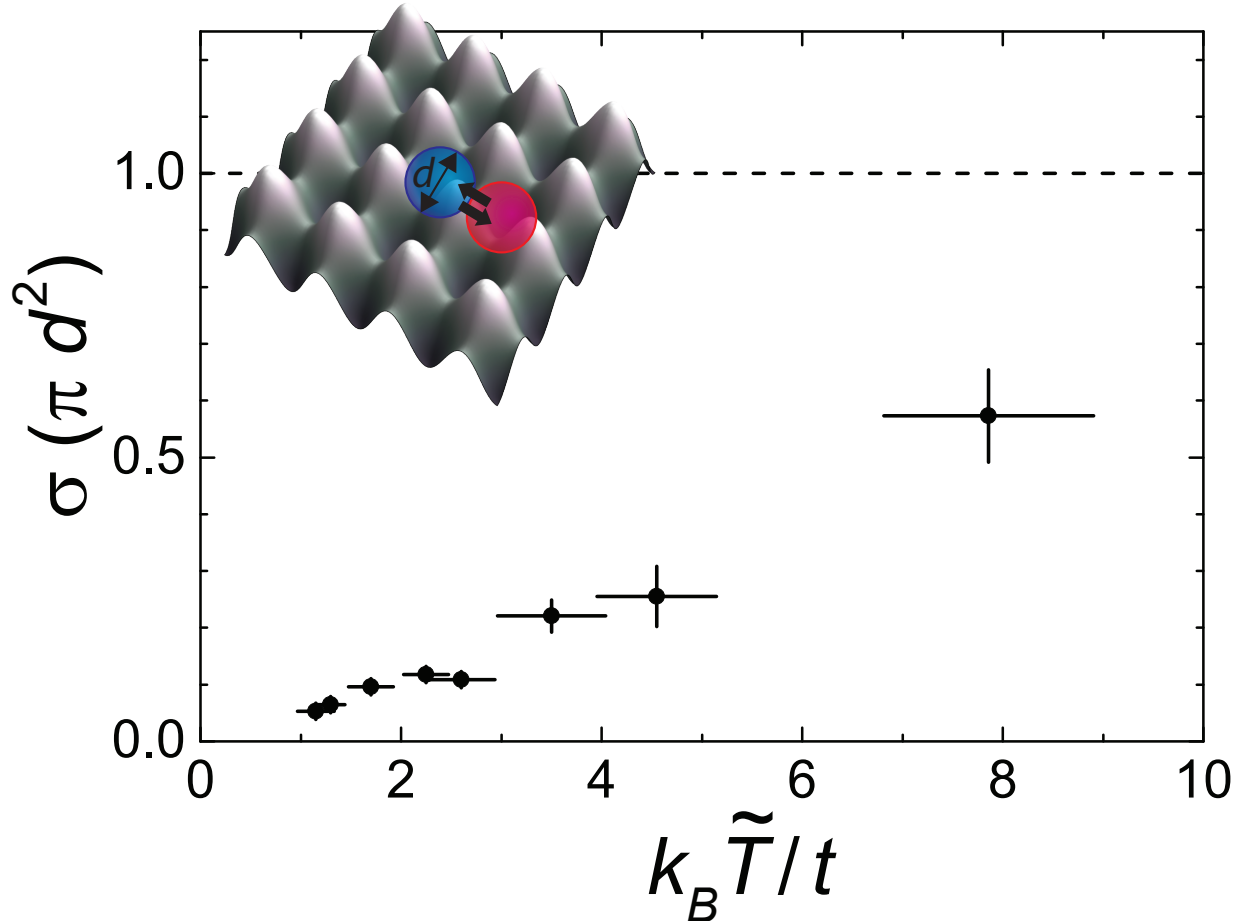


FIG. 4: Collision cross section. The collision cross section inferred from the measured τ and \tilde{T} is shown for the data in Fig. 3b. The vertical error bars are derived from the uncertainty in τ . The inset depicts the hard-sphere limit (achieved at unity on the vertical axis) associated with the lattice, where atoms collide as hard spheres with a diameter equal to the lattice spacing d .

The cross section determined using this approach increases approximately linearly with temperature, growing to $\sigma \approx 0.5\pi d^2$ at the highest temperature we sample, where πd^2 is the collision cross section for hard spheres with diameters equal to the lattice spacing. For all temperatures, the cross section is significantly larger than that for free ^{40}K atoms $4\pi (170a_0)^2 \approx 0.002d^2$, where a_0 is the Bohr radius [30]. Furthermore, the free-particle cross section is largely energy and temperature independent for the small magnetic field we apply

and the range of temperatures sampled in Fig. 4 [29]. The temperature dependence evident in Figs. 3b and 4 must therefore arise from strong correlation effects.

It is remarkable that this relatively simple physical scenario consisting of band structure and strong on-site interactions gives rise to behavior analogous to strange metal phenomena. Many of the complications present in solids, such as disorder, electron–phonon interactions, variable range hopping, and multi-orbital effects, are absent in this system, and are thus not necessary to generate an analog strange metal. Our experiments thus provide a well controlled benchmark that will constrain future theory of the metallic state in Hubbard models.

We acknowledge funding from the National Science Foundation (PHY 12-05548, PHY 15-05468) and Army Research Office (W911NF-12-1-00462), and we thank Erich Mueller (Cornell University) and Joseph Thywissen (University of Toronto) for helpful conversations.

-
- [1] G. D. Mahan, *Many-Particle Physics* (Springer US, 2000).
 - [2] A. J. Schofield, *Contemp. Phys.* **40**, 95 (1999).
 - [3] J. Bruin, H. Sakai, R. Perry, and A. Mackenzie, *Science* **339**, 804 (2013).
 - [4] S. A. Hartnoll and A. Karch, *Phys. Rev. B* **91**, 155126 (2015).
 - [5] O. Gunnarsson, M. Calandra, and J. Han, *Rev. Mod. Phys.* **75**, 1085 (2003).
 - [6] A. Damascelli, Z. Hussain, and Z.-X. Shen, *Rev. Mod. Phys.* **75**, 473 (2003).
 - [7] J. Zaanen, S. Chakravarty, T. Senthil, P. Anderson, P. Lee, J. Schmalian, M. Imada, D. Pines, M. Randeria, C. Varma, et al., *Nat. Phys.* **2**, 138 (2006).
 - [8] J. McGreevy, *Physics* **3**, 83 (2010).
 - [9] P. W. Anderson, *Nat. Phys.* **2**, 626 (2006).
 - [10] C. V. Johnson and P. Steinberg, *Phys. Today* **63**, 29 (2010).
 - [11] H. Liu, *Physics Today* **65**, 68 (2012).
 - [12] D. Jaksch, C. Bruder, J. I. Cirac, C. W. Gardiner, and P. Zoller, *Phys. Rev. Lett.* **81**, 3108 (1998).
 - [13] T. Esslinger, *Annu. Rev. Condens. Matter Phys.* **1**, 129 (2010).
 - [14] M. Lewenstein, A. Sanpera, V. Ahufinger, B. Damski, A. Sen, and U. Sen, *Advances in Physics* **56**, 243 (2007).

- [15] Y. Sagi, T. E. Drake, R. Paudel, R. Chapurin, and D. S. Jin, Phys. Rev. Lett. **114**, 075301 (2015).
- [16] U. Schneider, L. Hackermüller, J. P. Ronzheimer, S. Will, S. Braun, T. Best, I. Bloch, E. Demler, S. Mandt, D. Rasch, et al., Nat. Phys. **8**, 213 (2012).
- [17] C. Cao, E. Elliott, J. Joseph, H. Wu, J. Petricka, T. Schäfer, and J. E. Thomas, Science **331**, 58 (2011).
- [18] A. Sommer, M. Ku, G. Roati, and M. W. Zwierlein, Nature **472**, 201 (2011).
- [19] A. M. Rey, G. Pupillo, C. W. Clark, and C. J. Williams, Phys. Rev. A **72**, 033616 (2005).
- [20] D. McKay, M. White, and B. DeMarco, Phys. Rev. A **79**, 063605 (2009).
- [21] Materials and methods are available as supplementary materials.
- [22] B. DeMarco, S. Papp, and D. Jin, Phys. Rev. Lett. **86**, 5409 (2001).
- [23] S. Gensemer and D. Jin, Phys. Rev. Lett. **87**, 173201 (2001).
- [24] F. Reif, *Fundamentals of statistical and thermal physics* (McGraw-Hill, 1965).
- [25] S. A. Hartnoll, Nat. Phys. **11**, 54 (2015).
- [26] C. Varma, P. B. Littlewood, S. Schmitt-Rink, E. Abrahams, and A. Ruckenstein, Phys. Rev. Lett. **63**, 1996 (1989).
- [27] S. A. Hartnoll, J. Polchinski, E. Silverstein, and D. Tong, J. High Energy Phys. **2010**, 1 (2010).
- [28] T. Faulkner, N. Iqbal, H. Liu, J. McGreevy, and D. Vegh, Science **329**, 1043 (2010).
- [29] B. DeMarco, J. L. Bohn, J. P. Burke, M. Holland, and D. S. Jin, Phys. Rev. Lett. **82**, 4208 (1999).
- [30] S. Falke, H. Knöckel, J. Friebe, M. Riedmann, E. Tiemann, and C. Lisdat, Phys. Rev. A **78**, 012503 (2008).